RSC Advances

PAPER

View Article Online
View Journal | View Issue

Cite this: *RSC Adv.*, 2021, **11**, 21127

The enhanced visible-light-induced photocatalytic activities of bimetallic Mn–Fe MOFs for the highly efficient reductive removal of Cr(VI)†

Zohreh Garazhian, Alireza Farrokhi,* Abdolreza Rezaeifard,* Maasoumeh Jafarpour and Rouhollah Khani

Received 12th March 2021
Accepted 23rd May 2021

DOI: 10.1039/d1ra01986d

rsc.li/rsc-advances

The photocatalytic efficiencies of bimetallic MOFs, namely STA-12-Mn–Fe, for the reductive removal of Cr(VI) were explored. The best effective variable values were obtained and correlation between the response and influential variables was optimized *via* experimental design methodology. Complete Cr(VI) removal was achieved under natural sunlight and fluorescent 40 W lamp radiation at pH 2, with an initial Cr(VI) concentration of 20 mg L^{-1}, and 10 mg of photocatalyst within 30 min. A pseudo-first-order rate constant of 0.132 min^{-1} at $T = 298$ K was obtained for the Cr(VI) reduction reaction. The title catalysts revealed high performance in the visible region based on photoefficiency measurements, while improved activity was observed compared to the corresponding single-metal MOFs under natural sunlight, highlighting the synergistic effect between the two metal ions. Trapping experiment results proved that direct electron transfer is the main pathway during the photocatalytic Cr(VI) reduction process.

1. Introduction

Polluted wastewaters and groundwater from rivers, lakes, and seas are of special interest to researchers working on water depollution and environmental protection.[1] Indeed, water quality standards and rules of pollutant prevention have become stricter in many societies. The search for environmental remediation as well as clean, sustainable, and renewable energy has induced profuse research interest in photocatalysis, which is a powerful method for utilization of sunlight as the main and sustainable energy source.[2] The developing fields of photocatalysis include CO_2 reduction into organic fuels, water splitting for H_2 generation, and removal of environmental pollutants.[3–5] Recent advancements in photocatalysis mostly emphasize the procedures to increase light absorption, prevent hole–electron recombination, and enhance the charge exploitation of the photocatalyst to optimize the light energy conversion efficiency.[6,7] Owing to the vast utilization of light, heterogeneous photocatalysis has to be an efficient and green method.[8] Due to the instantaneous charge separation, the moderate tunability, and chemical instability, the application of prevalent semiconductors as photocatalysts is restricted, and researches are concentrated on finding novel, tunable and efficient photocatalysts.[9]

Compared with conventional inorganic semiconductors, metal–organic frameworks (MOFs), a category of porous materials built from metal ions and organic linkers, have been lately considered as photocatalysts owing to their striking advantages in the following features: (1) the high porosity of MOFs permits the availability of catalytic sites and accelerates the transport of reactants; (2) the tunability of MOFs creates an excellent opportunity to develop the light response over the visible range; (3) the crystalline nature of MOFs limits the structural defects, which are centers of charge recombination, and greatly reduces hole–electron recombination; (4) the well-defined MOF structures have great promise in the realizing of structure–activity relations.[10–13]

Mixed-metal MOFs having more than one metal in the chemical structure are particular instances of structure tunability in MOFs.[14] These MOFs provide features in terms of multi-functionality and tuning of the structure to a specific application. Due to the probable synergistic effects that derive from the existence of two or more metals, mixed-metal MOFs can display higher efficiency compared to single-metal MOFs.[12] Mixed-metal MOFs can also have better stability, increasing the strength of the framework, making them adequate for broad applications.[15] Because of these merits, interesting studies on the catalytic removal of several organic and inorganic pollutants with MOF-based photocatalysts have recently been reported.[16,17] However, these researches are limited to MOFs made of carboxylic acid and imidazolate ligands, and those containing phosphonic acid ligands have been rarely used.[18–20]

Department of Chemistry, Faculty of Science, University of Birjand, Birjand 97179-414, Iran. E-mail: afarrokhi@birjand.ac.ir; rrezaeifard@birjand.ac.ir

† Electronic supplementary information (ESI) available. See DOI: 10.1039/d1ra01986d

Encouraged by the promising results on the photocatalytic performance of phosphonate-based MOFs in dye degradation,[19,20] herein, we extend our research toward photocatalytic removal of Cr(VI) as a notorious environmental pollutant, using phosphonate-based bimetallic STA-12-Mn–Fe MOFs with various amounts of Fe(II) and Mn(II) ions under natural sunlight and fluorescent lamp radiation. The CCD (central composite design) method was used to optimize the main factors in the photocatalytic reaction (Cr(VI) concentration, pH, irradiation time and photocatalyst mass). The title MOFs exhibited high photocatalytic efficiency and excellent reusability during Cr(VI) reduction under natural and artificial irradiation. Also, a plausible photocatalytic mechanism is suggested based on a set of scavenging experiments.

2. Experimental

2.1. Reagents

All reagents were used as received and without further purification. Ferrous chloride tetrahydrate ($FeCl_2 \cdot 4H_2O$), manganese(II) acetate tetrahydrate ($Mn(OAc)_2 \cdot 4H_2O$), potassium dichromate ($K_2Cr_2O_7$), piperazine, formaldehyde, H_2SO_4, ammonium oxalate ($(NH_4)_2C_2O_4$), ethanol, methanol, citric acid, formic acid, KOH and Na_2EDTA were purchased from Merck. Distilled water was used for the preparation of the solutions.

2.2. Preparation of the organic linker (H_4L)

An organic ligand with a structure of *N*,*N*′-piperazinebis-(methylene)bisphosphonic acid, $H_2O_3P–CH_2–NC_4H_8N–CH_2–PO_3H_2$, was prepared according to a reported method,[21] and was characterized by NMR and IR (ESI, Fig. S1–S4†).

2.3. Preparation of the bimetallic MOFs

MOFs with the structure of STA-12-Mn–Fe containing various amounts of iron and manganese ions were synthesized and characterized according to a method reported previously[19] (ESI, Table S1 and Fig. S5–S9†).

2.4. Instrumentation

HANNA (HI 2211 pH/ORP meter) and Hettich (ZENTRIFUGEN ROTOFIX 32 A) centrifuge devices were used for sample separation. The IR spectra were collected with a Shimadzu 800 FT-IR spectrometer. Design-Expert software version 10.0 (StatEase Inc., Minneapolis, MN, USA) was applied for experimental design analysis. PXRD data were collected using an X'Pert PRO diffractometer with Cu-Kα radiation. Elemental analyses were carried out with ICP-AES (PerkinElmer Optima 7300 DV). Also, energy-dispersive spectroscopy mapping was used to study the distribution of elements in the surface of the as-prepared MOFs. UV/visible DRS spectra were recorded with an Avantes spectrometer (Avaspec-2048-TEC). NMR spectra were recorded with a Bruker (Avance DRS) 500 spectrometer.

2.5. Procedure for Cr(VI) photoreduction

The photocatalytic reduction of Cr(VI) was performed in a glass beaker (50 mL) containing 40 mL of a solution of Cr(VI) (20 mg L^{-1}) adjusted to pH = 2 using H_2SO_4 (2 M) under stirring. 5 mg of hole scavenger reagent and 10 mg of STA-12-Mn–Fe were added into the beaker. The reaction mixture was stirred for 40 min in the dark, to afford adsorption equilibrium between the catalyst surface and reactants. After that, the reaction suspension was exposed to natural sunlight radiation under stirring on sunny days in May between 10:00 AM and 2:00 PM,[22] and also under a fluorescent lamp (CFL) at a distance of 10 cm. At certain periods, 2 mL of the reaction mixture was extracted and centrifuged to eliminate the MOF. The amount of Cr(VI) removal was analyzed by an Analytik Jena SPECORD PLUS UV-visible spectrophotometer and specified at 540 nm using the DPC (diphenyl carbazide) method.[23]

2.6. Effective species evaluation tests

To elucidate the active species involved in the photocatalytic Cr(VI) reduction, trapping tests were done with diverse types of scavengers. Therefore, chloroform (as $O_2^{\bullet-}$ scavenger), methanol (as $^{\bullet}OH$ scavenger) and $AgNO_3$ (as electron scavenger) were added to the reaction during the catalytic experiments.

2.7. Procedure for photoefficiency assessments

A fluorescent 40 W lamp was utilized as an artificial visible radiation source equipped with cut-off filters: a solution mixture of $KMnO_4$, MB (methylene blue) and phenol red to irradiate at $\lambda \approx 760$ nm with lux = 1093;[24] a mixture of $KMnO_4$, $Cu(NO_3)_2$ and $KCrO_4$ to illuminate at $\lambda \approx 600$ nm with lux = 4895; a green filter (Leybold Heraeus GmbH 46807) to illuminate at $\lambda \approx 530$ nm with lux = 7145; a blue filter (Leybold Heraeus GmbH 46811) to illuminate at $\lambda \approx 450$ nm with lux = 5773; and a solution of MB to irradiate at $\lambda \approx 415$ nm with lux = 2786 were used as filters in this research. The reduction of Cr(VI) was accomplished based on the aforementioned method.

3. Results and discussion

3.1. Primary assessment of the photocatalytic activities

Knowing that Cr(VI) reduction is favored at low pH conditions,[25] the preliminary tests for Cr(VI) reduction were performed at pH = 2 at ambient temperature in darkness and sunlight, in the absence and presence of catalyst and with ethanol as hole scavenger (for more information on catalyst identification and data analysis, see ESI† and ref. 19). In the absence of light, photocatalyst and hole scavenger, no Cr(VI) removal occurred, evidence that STA-12-Mn–Fe acts as a photocatalyst and MOF, light and hole scavenger are vital for triggering the Cr(VI) reduction (Fig. 1a). Additional experiments were also conducted in the presence of various hole scavengers such as EDTA, citric acid, formic acid, ethanol, methanol and ammonium oxalate under the same conditions (Fig. 1b). Ammonium oxalate demonstrated the most efficient hole scavenging activity for photoreduction of Cr(VI) with

bimetallic STA-12-Mn–Fe (50 : 50). This could be due to the capability of ammonium oxalate to rapidly adsorb on the MOF and so contribute effectively in the catalytic reaction. Also, oxalate ions are able to produce $CO_2^{\cdot}$ radicals, which can transfer electrons more efficiently to the holes of the photocatalyst.[26,27] Therefore, hole–electron recombination is reduced efficiently and more electrons are available for the reduction of Cr(VI). Based on these results, $(NH_4)_2C_2O_4$ was chosen for further investigations.

Further investigation showed that ammonium oxalate amount greater than 5 mg did not increase the efficiency of the Cr(VI) reduction process.

3.2. Experimental design and the development of a regression model equation

CCD[28] as a multivariate technique was used to avoid the requirement for a vast number of tests, which extremely increases the cost and required time. Also, this technique is predominantly used for modeling experiments, assessing the effective variables, and seeking optimal conditions of a process. The pH (A), concentration of Cr(VI) (B), amount of catalyst (C) and time of irradiation (D) were selected as the main variables. Thirty randomized experiments were designed based on the CCD in three blocks (each block has three replicates). The appropriate limits for the above parameters, symbols and units specified based on initial tests are presented in Table 1. The best correlation between the reduction percentage of Cr and input parameters was selected in terms of the following equation:

$$\begin{aligned}\text{Cr(VI) removal (\%)} = {} & +40.85 - 22.00 \times A - 13.09 \\ & \times B + 0.76 \times C + 1.89 \times D + 10.63 \\ & \times AB + 6.18 \times CD + 5.46 \\ & \times A^2 + 6.62 \times B^2 \end{aligned} \quad (1)$$

Table 1 Effective factors and their values in the CCD for Cr(VI) reduction

Factor	Symbol	Unit	$-\alpha$	-1	0	$+1$	$+\alpha$
pH	*A*	—	1	2	3	4	5
Cr(VI) conc.	*B*	mg	10	20	30	40	50
Amount of catalyst	*C*	mg	5	10	15	20	25
Time	*D*	min	10	30	50	70	90

Based on the variance analysis (ANOVA), the model was significant as well. The excellent predictability of the model was supported with the non-significant lack of fit ($P > 0.05$) (Table S2†). The R^2 values (0.97 and 0.96) are near to 1.0, confirming the goodness of the fit.

3.2.1. Appraisal of diagnostic and response surface plots. As shown in Fig. 2a, apparent dispersal in the collected data points is not observed, which is favorable and indicates the normal distribution of the data.[29] Comparative effects of all factors on the Cr(VI) reduction are depicted in the perturbation plot (Fig. 2b). A sharp curvature in the pH and Cr concentration curves demonstrates that the Cr(VI) reduction was highly sensitive to these factors.[30] The approximately flat lines of the time and amount of catalyst show a small sensitivity of the Cr(VI) reduction to variation in these parameters. Therefore, Cr(VI) concentration and pH are the critical factors in this research. The experimental and predicted amounts are quite close to each other (Fig. 2c), confirming that the presented model correctly estimates the correlation between the influential factors on the response.[31]

The simultaneous effect of pH and Cr(VI) concentration on the reduction of Cr(VI) is depicted in the contour plots (Fig. 3a) and three-dimensional response surface (Fig. 3b). These plots demonstrate that the removal of Cr(VI) increases with a decrease

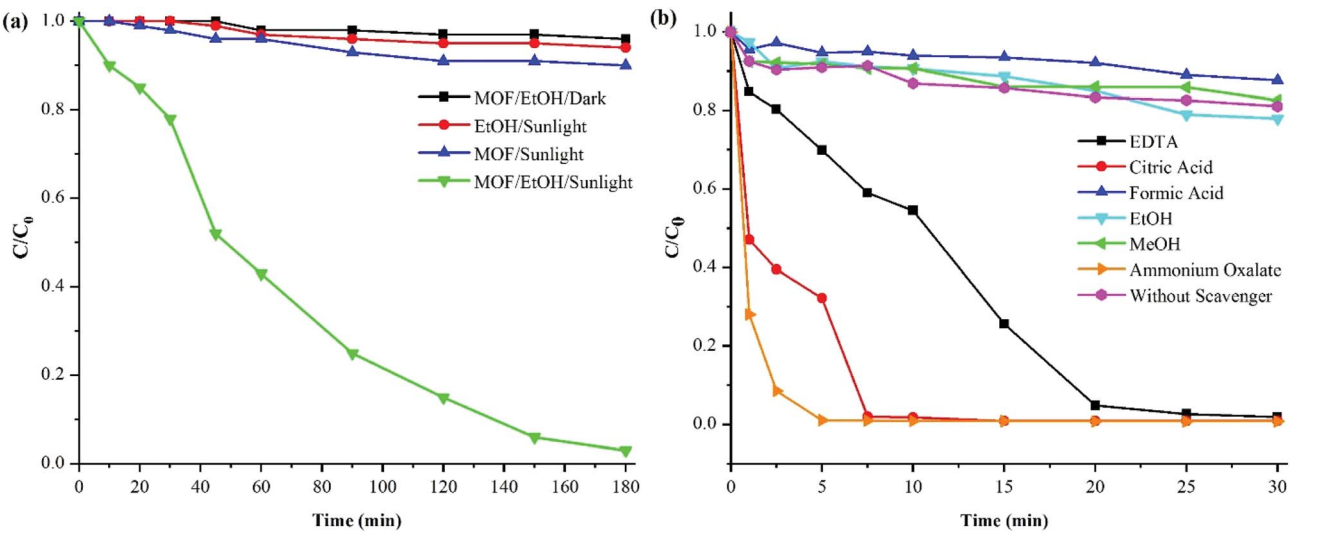

Fig. 1 (a) The initial evaluation of different variables in the photocatalytic reduction of Cr(VI). (b) The effects of various hole scavengers in the photocatalytic reaction with STA-12-Mn–Fe (50 : 50).

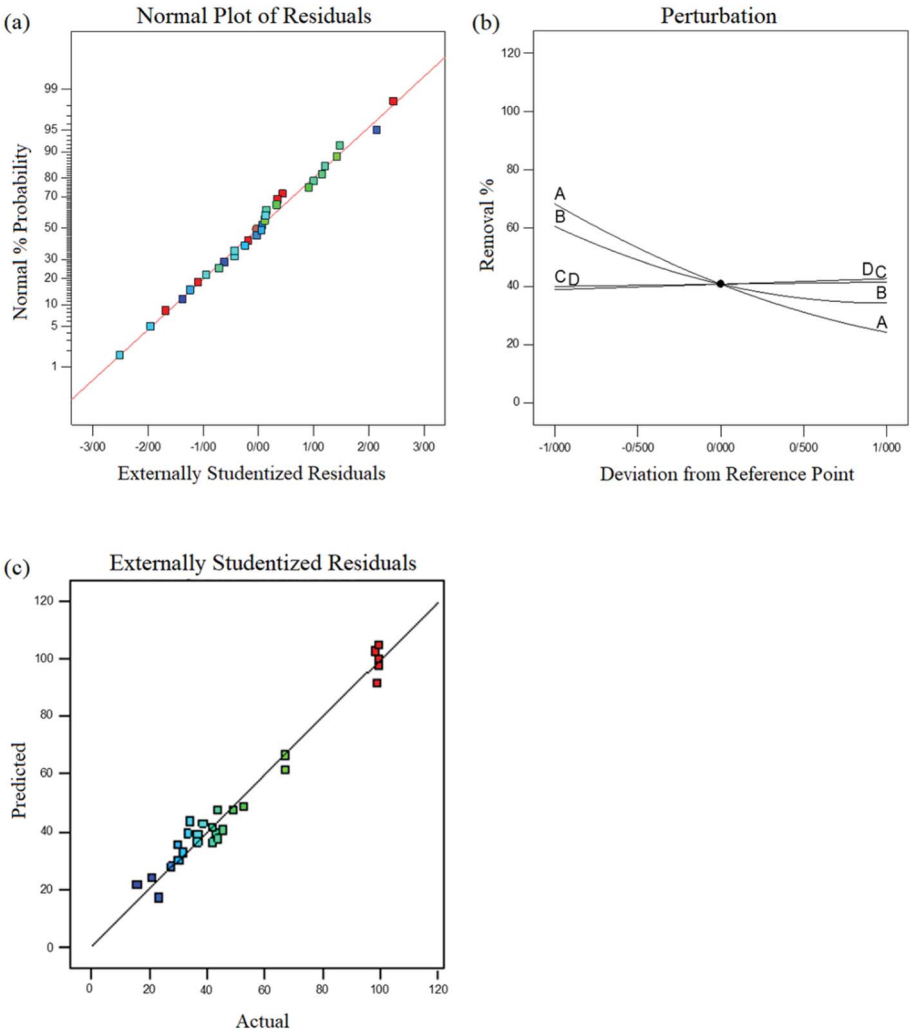

Fig. 2 (a) Residuals in the normal probability plot. (b) A perturbation plot for the removal of Cr(VI) over STA-12-Mn–Fe (50 : 50). (c) Actual data *vs.* predicted data for Cr(VI) reduction.

in the pH. The inverse relation between reduction performance and pH could be the result of the redox process in eqn (2):

$$Cr_2O_7^{2-} + 6e^- + 14H^+ \rightarrow 7H_2O + 2Cr^{3+} \quad (2)$$

Besides, the maximum removal was observed when the concentration of Cr(VI) was 20 mg L^{-1}. With regard to the plots, 3D plots (Fig. 3c–f) and Table S2,† the interactions between other factors such as the time, pH, and amount of catalyst were not significant.

3.2.2. Optimized parameters for the reduction of Cr(VI). The desirability function approach (1.0 (very desirable) to 0.0 (undesirable)) was utilized to obtain the optimized reduction conditions. According to the desirability score of 1.00, maximum Cr(VI) removal was achieved for the following optimal conditions: pH = 2, concentration of Cr(VI) = 20 mg L^{-1}, amount of catalyst = 10 mg and time = 30 min. The results of 3 replicates at the defined optimal conditions have good proximity with predicted data. Moreover, our results revealed that changes in the molar ratio of Mn and Fe in the as-prepared bimetallic MOFs does not alter their efficiency and excellent performance for Cr(VI) removal was observed for all the ratios used in this work under both light sources (Fig. 4). Nevertheless, when we compared our results with those obtained when using single-metal MOFs STA-12-Fe, reported in our previous work,[32] an improved activity of bimetallic STA-12-Mn–Fe in the reductive removal of Cr(VI) under natural sunlight was observed (99% removal in 5 min against 98% removal in 20 min; Fig. 4). This can be attributed to the lower band gap and the synergy of Fe and Mn ions in STA-12-Mn–Fe.

3.3. Photochemical activity of STA-12-Mn–Fe

As mentioned in Section 3.1, performing a control reaction in the dark did not change the concentration of Cr(VI). Nevertheless, the reaction under natural sunlight showed complete removal of Cr(VI) in less than 30 min, demonstrating the visible

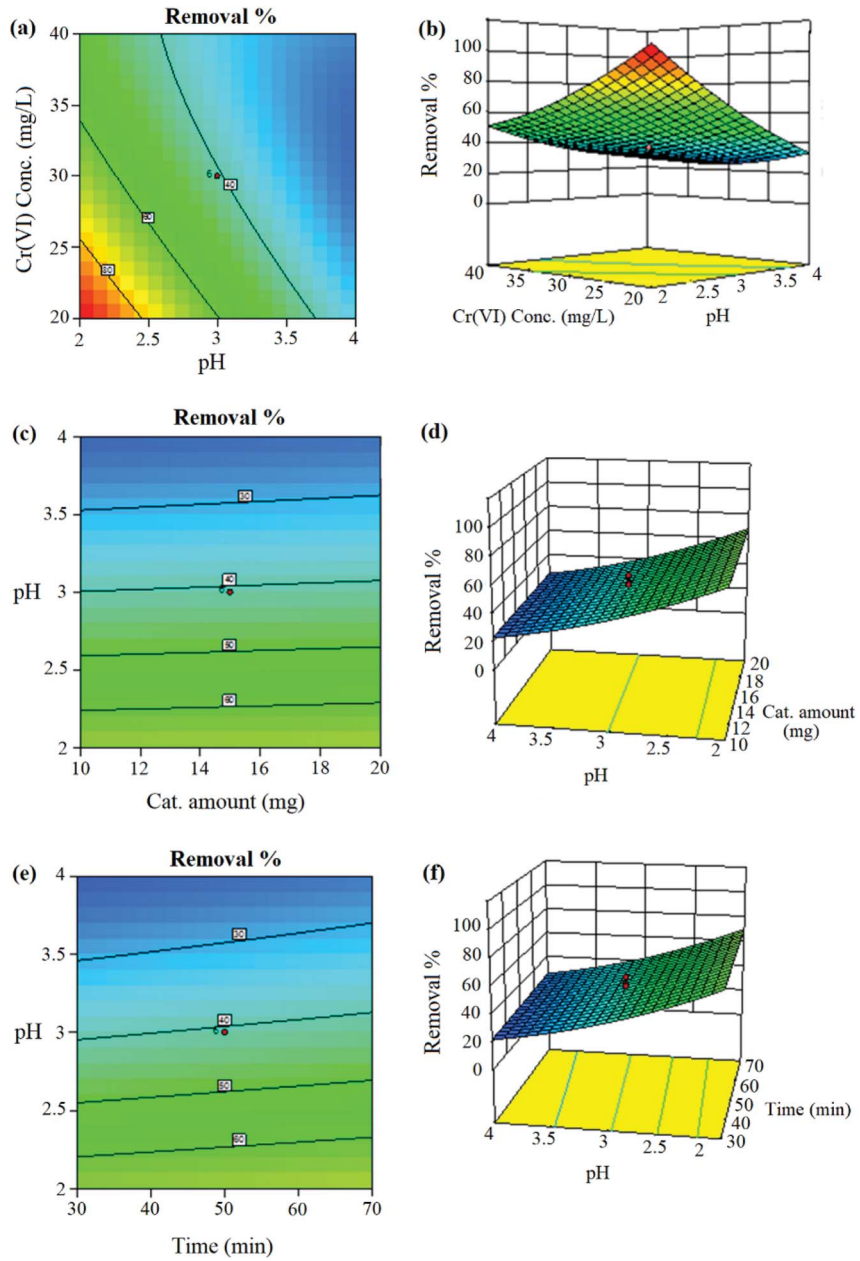

Fig. 3 Three-dimensional and contour plots for the removal of Cr(VI) showing the effects of (a and b) Cr(VI) concentration and pH, (c and d) pH and the amount of catalyst, and (e and f) pH and reaction time.

light activity of the photocatalyst. The optical properties of the prepared samples were assessed with UV-visible DRS (Fig. S5†). The band gaps of these samples, evaluated from the Tauc plots, are about 2.3 eV (insets of Fig. S5†). According to the band gap values, all of these MOFs could be visible light-sensitive photocatalysts. The effect of diverse visible-light wavelengths on Cr(VI) reduction with SAT-12-Mn–Fe (50 : 50) was explored under irradiation of a CFL lamp utilizing various filters (see Section 2.7). To specify whether the reduction reaction happened *via* a thermo-catalytic or a photo-induced process, the apparent quantum efficiency (AQE) as a useful tool was estimated by eqn (3):[33,34]

$$\text{AQE} = \text{no. reacted molecules/no. incident photons} \quad (3)$$

The values of AQE calculated for SAT-12-Fe–Mn (50 : 50) at different wavelengths of 415, 450, 530, 600, and 760 nm under CFL radiation reached 0.034, 0.013, 0.01, 0.003, and 0.004, respectively. These results are in good accord with the diffuse reflection spectra (Fig. 5), which confirm the visible-light activity of the MOFs under optimized conditions.

3.4. Kinetics analysis

The kinetic study of Cr(VI) photoreduction over STA-12-Mn–Fe (50 : 50) shows that the reaction follows the pseudo-first-order

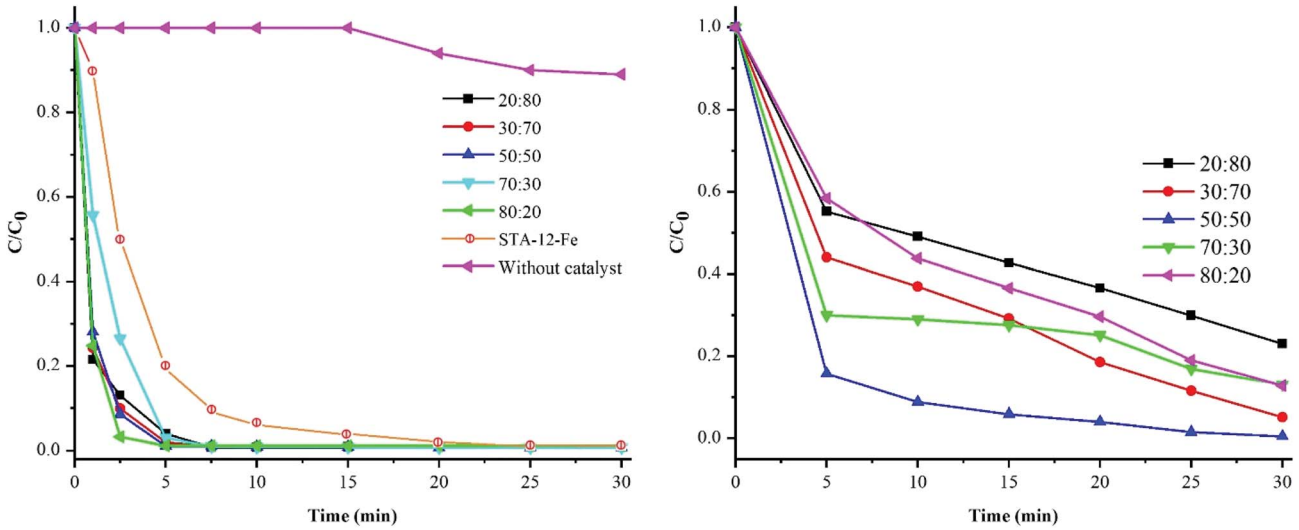

Fig. 4 Time-dependent Cr(VI) reduction under natural sunlight (left) and a CFL lamp (right) with various MOFs. Reaction conditions: 40 mL of Cr(VI) solution, 20 ppm; pH = 2; 5 mg of ammonium oxalate; 10 mg of catalyst.

kinetic model: $\ln(C/C_0) = k_{app} \times t$, where C_0 is the Cr(VI) initial concentration, C is the Cr(VI) concentration at time t, and k_{app} is the apparent rate constant, which is the slope of the plot depicted in Fig. 6. The value of k_{app} was determined to be 0.132 min^{-1} at $T = 300$ K by linear regression of the R^2 value of 0.9729 (Fig. 6).

3.5. Mechanism of photoassisted Cr(VI) reduction

Radical scavenging tests were performed to identify the active species in the photocatalytic reduction (Fig. 7). After that, a proposed mechanism for the process was elucidated. Among various scavengers, only $AgNO_3$ (e^- scavenger) extremely inhibits the Cr(VI) reduction. This finding suggests that the catalytic reaction proceeds solely through direct electron transfer from the MOF surface to Cr(VI) ions and other active species ($O_2^{\bullet -}$, h^+ and $^{\bullet}OH$) do not affect the process.

The band gap (E_g) of STA-12-Mn–Fe (50 : 50) estimated by the Tauc plot (Fig. S5†) was found to be 2.3 eV. Furthermore, the

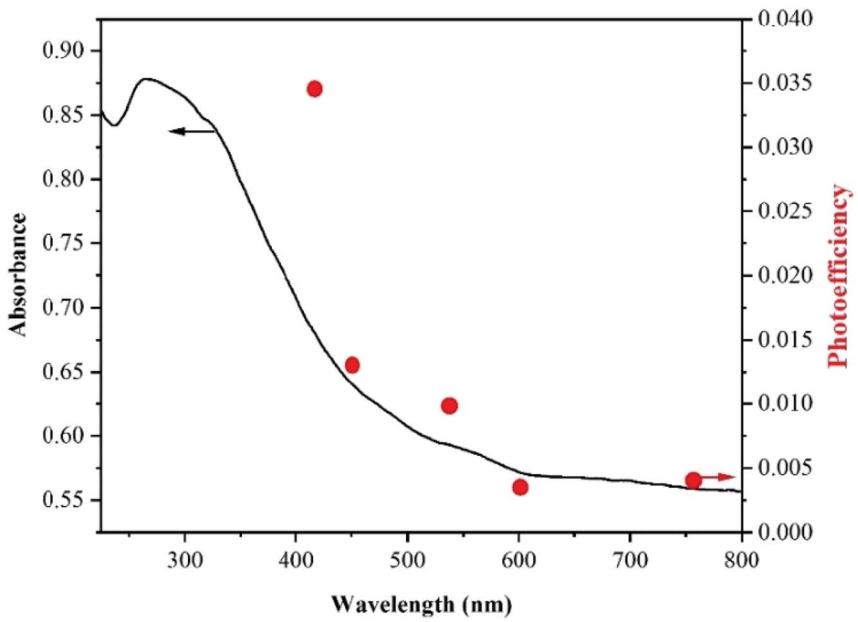

Fig. 5 The absorption spectrum of STA-12-Mn–Fe (50 : 50) (solid line) and action spectrum for the removal of Cr(VI) in the optimal situation under CFL radiation (red points).

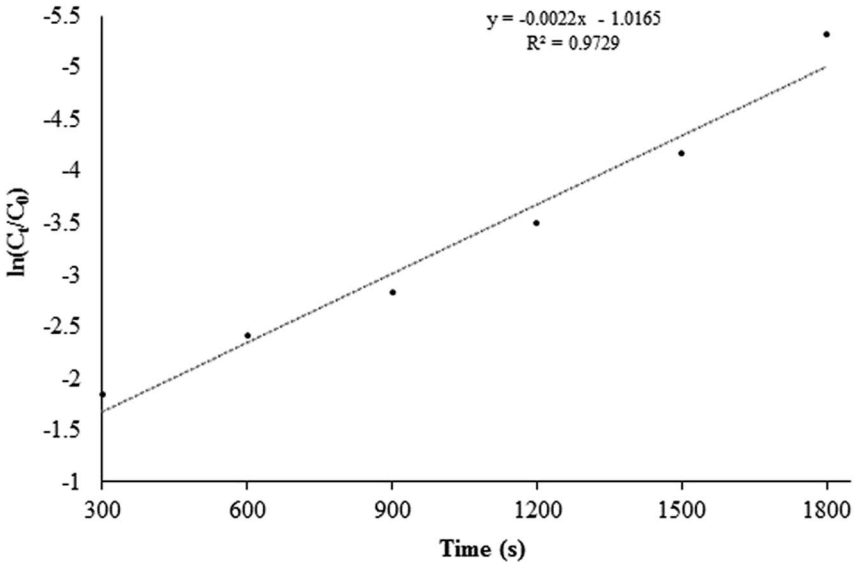

Fig. 6 A pseudo-first-order plot for photocatalytic Cr(VI) reduction catalyzed by STA-12-Mn–Fe (50 : 50).

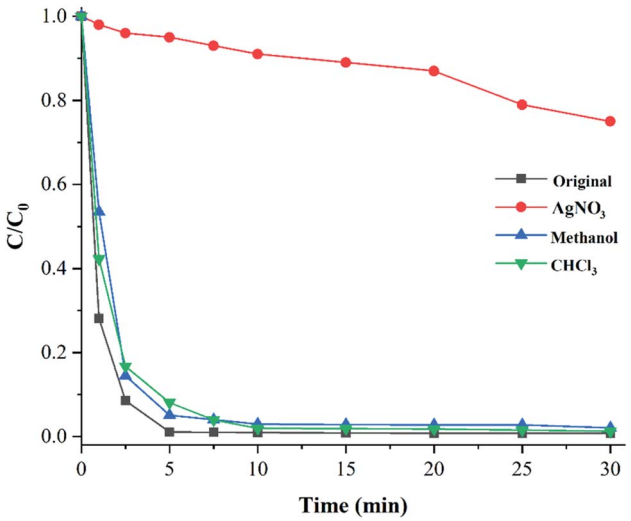

Fig. 7 Radical trapping tests in photocatalytic Cr(VI) reduction with STA-12-Mn–Fe (50 : 50) (amount of trapping agent = 10 mg).

conduction band (CB) and valence band (VB) positions of the photocatalyst were evaluated with the following equation:[35]

$$E_{CB} = E_0 + 0.059(pH_{PZC} - pH) - X - 0.5E_g \quad (4)$$

E_{CB} refers to the potential of the CB. The value of E_0 is 4.5 eV. pH_{PZC} (the isoelectric point of MOF) value is 4.6 (Fig. S7†). X (the bulk electronegativity of catalyst) demonstrates the geometric average of the absolute electronegativities of atoms in the MOF structure.[36] The value of X for STA-12-Mn–Fe (50 : 50) is 6.65 eV. Thus, the VB and CB potentials are calculated as −5.44 eV and −3.15 eV, respectively. As shown in Fig. 8, the CB of the photocatalyst is above the reduction potential of Cr(VI)[37] and the VB of MOF is below the oxidation potential of oxalate,[38] which are adequate for electron and hole transfer and confirm the photocatalytic ability of STA-12-Mn–Fe for removal of Cr(VI).

A likely mechanism for Cr(VI) removal under visible light by STA-12-Mn–Fe is depicted in Fig. 8. In the structure of STA-12 MOFs, the chains built from edge-shared MNO_5 octahedra are connected *via* organic linkers (H_4L).[39] It is noteworthy that the organic ligand in the catalyst structure is not visible light active. However, the metal-containing chains in the photocatalyst can absorb visible-light photons and produce hole–electron pairs. In the reaction mixture, Cr(VI) reacts with the electrons and the holes interact with oxalate ions as a scavenger. Thus, the hole–electron recombination is disrupted and Cr(VI) reduction proceeds efficiently.

3.6. Reusability and stability tests

The reusability tests for STA-12-Mn–Fe (50 : 50) in the Cr(VI) reduction reaction reveal that the photocatalytic efficiency of the MOF does not diminish after four runs and the catalyst remained stable during the reaction (Fig. S8†). Also, the PXRD and IR analyses show that the chemical structure of the photocatalyst has not altered after four consecutive catalytic processes (Fig. S9†). Furthermore, elemental analysis of the MOF after reaction demonstrated 1% and 0.5% decrease in Mn and Fe, respectively, confirming the durability of STA-12-Mn–Fe in the catalytic process.

To show the activity of this photocatalytic system, the results obtained for the reduction of Cr(VI) in the presence of STA-12(Fe) were compared with those reported for other MOFs under sunlight irradiation (Table 2). All parameters confirm that this photocatalytic system is highly efficient for the removal of Cr(VI) in comparison to other systems, including short reaction time, low catalyst loading, high removal percentage, using a sustainable light source, and conditions used.

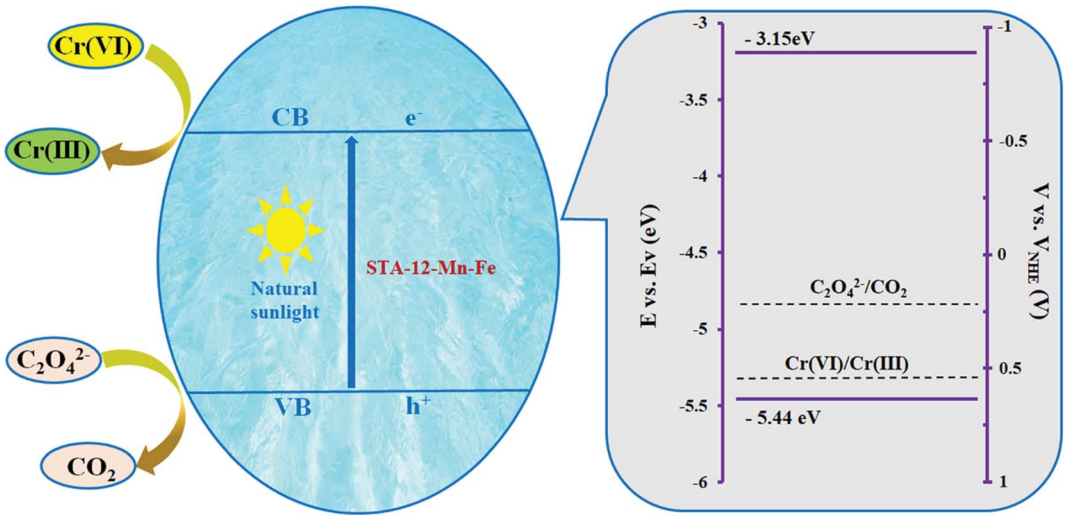

Fig. 8 A schematic diagram of Cr(VI) removal with the STA-12-Mn–Fe (50 : 50) photocatalyst under visible light irradiation.

Table 2 A comparison of the photocatalytic activity of STA-12(Fe) with that of other reported MOFs under sunlight irradiation[a]

MOF	Cr(VI)/MOF conc. (mg L^{-1})	Light/time for reduction (min)	Removal (%)	Ref.
MIL-53(Fe)	20/1000	SS/40	98	40
Zn-MOF	20/1000	NS/90	93	25
UiO-66-NH_2(Zr)	5/—	SS/120	98	41
NNU-36	10/375	SS/60	95	42
JLU-MOF60	80/400	SS/70	98	43
NNU-37	10/625	SS/110	91	44
STA-12(Fe)	30/250	NS/25	98	32
STA-12-Mn–Fe	20/250	NS/5	99	This work

[a] SS = simulated sunlight; NS = natural sunlight.

4. Conclusions

Five bimetallic MOFs with the formula STA-12-Mn–Fe have been applied to the visible-light-driven photocatalytic removal of Cr(VI). CCD was utilized for the modeling and optimization of the reaction parameters, including different influential factors, such as catalyst mass, irradiation time, Cr(VI) concentration, and pH. The results revealed that all ratios of Fe(II) and Mn(II) ions in the structure of STA-12-Mn–Fe provide efficient photocatalysis under natural and artificial visible light and present superior recyclability and stability for the reduction of Cr(VI). Due to the lower band gap and probable synergistic effects that derive from the existence of Mn and Fe ions, STA-12-Mn–Fe displays higher efficiency than single-metal MOFs. Radical scavenging tests show that direct electron transfer to Cr(VI) ions is the main mechanism during the photocatalytic reduction process. This research could provide a novel visible-light ARP for water treatment and it could expand the applications of bimetallic MOFs in environmental remediation and chemical synthesis.

Conflicts of interest

No conflicts of interest are declared by the authors.

Acknowledgements

The authors appreciate the support of the University of Birjand.

References

1 M. I. Stefan, *Advanced Oxidation Processes for Water Treatment - Fundamentals and Applications*, IWA Publishing, London, UK, 2018.
2 S. J. Phang, V. L. Wong, L. L. Tan and S. P. Chai, Recent advances in homojunction-based photocatalysis for sustainable environmental remediation and clean energy generation, *Appl. Mater. Today*, 2020, **20**, 100741.
3 M. Regue, S. Kumar and S. Eslava, *Heterogeneous Catalysis for Energy Applications*, 2020, p. 80.
4 F. Tian, S. Geng, L. He, Y. Huang, A. Fauzi, W. Yang, Y. Liu and Y. Yu, Interface engineering: PSS-PPy wrapping amorphous Ni–Co–P for enhancing neutral-pH hydrogen evolution reaction performance, *Chem. Eng. J.*, 2021, **417**, 129232.
5 X. Liu, H. Liu, Y. Wang, W. Yang and Y. Yu, Nitrogen-rich g-C_3N_4@AgPd Mott–Schottky heterojunction boosts photocatalytic hydrogen production from water and

tandem reduction of NO_3^- and NO_2^-, *J. Colloid Interface Sci.*, 2021, **581**, 619–626.

6 L. Ran, J. Hou, S. Cao, Z. Li, Y. Zhang, Y. Wu, B. Zhang, P. Zhai and L. Sun, Defect engineering of photocatalysts for solar energy conversion, *Sol. RRL*, 2020, **4**, 1900487.

7 Y. Wang, S. Bao, Y. Liu, W. Yang, Y. Yu, M. Feng and K. Li, Efficient photocatalytic reduction of Cr(VI) in aqueous solution over CoS_2/g-C_3N_4-RGO nanocomposites under visible light, *Appl. Surf. Sci.*, 2020, **510**, 145495.

8 *Heterogeneous Photocatalysis*, ed. Muñoz-Batista, M. J., Navarrete Muñoz, A. and Luque, R., Topics in Current Chemistry Collections, Springer, 2020.

9 S. Younis and K.-H. Kim, Heterogeneous photocatalysis scalability for environmental remediation: opportunities and challenges, *Catalysts*, 2020, **10**, 1109.

10 A. Dhakshinamoorthy, Z. Li and H. Garcia, Catalysis and photocatalysis by metal organic frameworks, *Chem. Soc. Rev.*, 2018, **47**, 8134–8172.

11 X. Gong, Y. Shu, Z. Jiang, L. Lu, X. Xu, C. Wang and H. Deng, Metal–organic frameworks for the exploitation of distance between active sites in efficient photocatalysis, *Angew. Chem., Int. Ed.*, 2020, **59**, 5326–5331.

12 C. W. Huang, V. H. Nguyen, S. R. Zhou, S. Y. Hsu, J. X. Tan and K. C. W. Wu, Metal–organic frameworks: preparation and applications in highly efficient heterogeneous photocatalysis, *Sustainable Energy Fuels*, 2020, **4**, 504–521.

13 T. Zhang, Y. Jin, Y. Shi, M. Li, J. Li and C. Duan, Modulating photoelectronic performance of metal–organic frameworks for premium photocatalysis, *Coord. Chem. Rev.*, 2019, **380**, 201–229.

14 S. Abednatanzi, P. Gohari Derakhshandeh, H. Depauw, F. X. Coudert, H. Vrielinck, P. Van Der Voort and K. Leus, Mixed-metal metal-organic frameworks, *Chem. Soc. Rev.*, 2019, **48**, 2535–2565.

15 J. Li, P. M. Bhatt, J. Li, M. Eddaoudi and Y. Liu, Recent progress on microfine design of metal–organic frameworks: structure regulation and gas sorption and separation, *Adv. Mater.*, 2020, 2002563.

16 X. Zhang, J. Wang, X. X. Dong and Y. K. Lv, Functionalized metal–organic frameworks for photocatalytic degradation of organic pollutants in environment, *Chemosphere*, 2020, **242**, 125144.

17 Q. Wang, Q. Gao, A. M. Al-Enizi, A. Nafady and S. Ma, Recent advances in MOF-based photocatalysis: environmental remediation under visible light, *Inorg. Chem. Front.*, 2020, **7**, 300–339.

18 T. Zeng, D. Shi, Q. Cheng, G. Liao, H. Zhou and Z. Pan, Construction of novel phosphonate-based MOF/P-TiO_2 heterojunction photocatalysts: enhanced photocatalytic performance and mechanistic insight, *Environ. Sci.: Nano*, 2020, **7**, 861–879.

19 A. Farrokhi, F. Feizpour and M. Asaadzadeh, Degradation of hazardous organic dyes with solar-driven advanced oxidation process catalyzed by the mixed metal–organic frameworks, *Appl. Organomet. Chem.*, 2019, **33**, e4928.

20 A. Farrokhi, M. Jafarpour and M. Alipour, Solar-driven advanced oxidation process catalyzed by metal–organic frameworks for water depollution, *Polyhedron*, 2019, **170**, 325–333.

21 A. Farrokhi, M. Jafarpour and R. Najafzade, Phosphonate-based metal–organic frameworks as robust heterogeneous catalysts for TBHP oxidation of benzylic alcohols, *Catal. Lett.*, 2017, **147**, 1714–1721.

22 A. A. Sabziparvar, A simple formula for estimating global solar radiation in central arid deserts of Iran, *Renewable Energy*, 2008, **33**, 1002–1010.

23 A. Idris, N. Hassan, R. Rashid and A. F. Ngomsik, Kinetic and regeneration studies of photocatalytic magnetic separable beads for chromium(VI) reduction under sunlight, *J. Hazard. Mater.*, 2011, **186**, 629–635.

24 Z. Garazhian, A. Rezaeifard, M. Jafarpour and A. Farrokhi, $\{Mo_{72}Fe_{30}\}$ nanoclusters for the visible-light-driven photocatalytic degradation of organic dyes, *ACS Appl. Nano Mater.*, 2020, **3**, 648–657.

25 H. Kaur, S. Sinha, V. Krishnan and R. R. Koner, Photocatalytic reduction and recognition of Cr(VI): new Zn(II)-based metal–organic framework as catalytic surface, *Ind. Eng. Chem. Res.*, 2020, **59**, 8538–8550.

26 L. G. Dodson, M. C. Thompson and J. M. Weber, Characterization of intermediate oxidation states in CO_2 activation, *Annu. Rev. Phys. Chem.*, 2018, **69**, 231.

27 X. B. Wang, X. Yang, J. B. Nicholas and L. S. Wang, Photodetachment of hydrated oxalate dianions in the gas phase, $C_2O_4^{2-}(H_2O)n$ (n = 3–40): from solvated clusters to nanodroplet, *J. Chem. Phys.*, 2003, **119**, 3631–3640.

28 J. E. Reece, S. N. Deming and S. L. Morgan, Experimental design: a chemometric approach, *Am. Stat.*, 1994, **48**, 172.

29 D. Vildozo, C. Ferronato, M. Sleiman and J. M. Chovelon, Photocatalytic treatment of indoor air: optimization of 2-propanol removal using a response surface methodology (RSM), *Appl. Catal., B*, 2010, **94**, 303–310.

30 H. L. Liu and Y. R. Chiou, Optimal decolorization efficiency of reactive red 239 by UV/TiO_2 photocatalytic process coupled with response surface methodology, *Chem. Eng. J.*, 2005, **112**, 173–179.

31 R. Khani, S. Sobhani and T. Yari, Magnetic dispersive micro solid-phase extraction of trace rhodamine B using imino-pyridine immobilized on iron oxide as nanosorbent and optimization by Box–Behnken design, *Microchem. J.*, 2019, **146**, 471–478.

32 A. Farrokhi, F. Bivareh, S. Dejbakhshpour and A. Z. Moghaddam, Insight into the photocatalytic properties of phosphonate-based metal–organic frameworks for reduction of Cr(VI) and synergistic elimination of organic dyes under natural sunlight, *Appl. Organomet. Chem.*, 2020, **34**, e5938.

33 B. Subash, B. Krishnakumar, M. Swaminathan and M. Shanthi, Synthesis and characterization of cerium–silver co-doped zinc oxide as a novel sunlight-driven photocatalyst for effective degradation of reactive red 120 dye, *Mater. Sci. Semicond. Process.*, 2013, **16**, 1070–1078.

34 X. Li, C. Chen and J. Zhao, Mechanism of photodecomposition of H_2O_2 on TiO_2 surfaces under visible light irradiation, *Langmuir*, 2001, **17**, 4118–4122.

35 X. Yong and M. A. A. Schoonen, The absolute energy positions of conduction and valence bands of selected semiconducting minerals, *Am. Mineral.*, 2000, **85**, 543–556.
36 R. G. Pearson, Absolute electronegativity and hardness: application to inorganic chemistry, *Inorg. Chem.*, 1988, **27**, 734–740.
37 X. Wang, S. O. Pehkonen and A. K. Ray, Removal of aqueous Cr(VI) by a combination of photocatalytic reduction and coprecipitation, *Ind. Eng. Chem. Res.*, 2004, **43**, 1665–1672.
38 J. A. Dean, *Lange's Chemistry Handbook*, 15th edn, 1999.
39 J. A. Groves, S. R. Miller, S. J. Warrender, C. Mellot-Draznieks, P. Lightfoot and P. A. Wright, The first route to large pore metal phosphonates, *Chem. Commun.*, 2006, 3305–3307.
40 R. Liang, F. Jing, L. Shen, N. Qin and L. Wu, MIL-53(Fe) as a highly efficient bifunctional photocatalyst for the simultaneous reduction of Cr(VI) and oxidation of dyes, *J. Hazard. Mater.*, 2015, **287**, 364.
41 X. D. Du, X. H. Yi, P. Wang, W. Zheng, J. Deng and C. C. Wang, Robust photocatalytic reduction of Cr(VI) on UiO-66-NH_2(Zr/Hf) metal–organic framework membrane under sunlight irradiation, *Chem. Eng. J.*, 2019, **356**, 393–399.
42 H. Zhao, Q. Xia, H. Xing, D. Chen and H. Wang, Construction of pillared-layer MOF as efficient visible-light photocatalysts for aqueous Cr(VI) reduction and dye degradation, *ACS Sustainable Chem. Eng.*, 2017, **5**, 4449–4456.
43 J. Liu, Y. Ye, X. Sun, B. Liu, G. Li, Z. Liang and Y. Liu, A multifunctional Zr(IV)-based metal–organic framework for highly efficient elimination of Cr(VI) from the aqueous phase, *J. Mater. Chem. A*, 2019, **7**, 16833–16841.
44 Z. Guo, H. Zhao, X. Liu, X. Liang, H. Wei, Y. Mei and H. Xing, Construction of visible-light-responsive metal–organic framework with pillared structure for dye degradation and Cr(VI) reduction, *Appl. Organomet. Chem.*, 2020, **34**, e5487.